The Journal of Chemical Physics

RESEARCH ARTICLE | MAY 12 2021

# Structural and topological changes across the liquid–liquid transition in water

**Special Collection:** JCP Editors' Choice 2021

Riccardo Foffi ; John Russo ; Francesco Sciortino



*J. Chem. Phys.* 154, 184506 (2021)
https://doi.org/10.1063/5.0049299

The Journal of Chemical Physics ARTICLE scitation.org/journal/jcp

# Structural and topological changes across the liquid–liquid transition in water

Cite as: J. Chem. Phys. 154, 184506 (2021); doi: 10.1063/5.0049299
Submitted: 3 March 2021 • Accepted: 20 April 2021 •
Published Online: 12 May 2021



Riccardo Foffi, John Russo, and Francesco Sciortino[a)]

## AFFILIATIONS

Department of Physics, Sapienza Università di Roma, Piazzale Aldo Moro, 2, 00185 Rome, Italy

[a)]Author to whom correspondence should be addressed: francesco.sciortino@uniroma1.it

## ABSTRACT

It has recently been shown that the TIP4P/Ice model of water can be studied numerically in metastable equilibrium at and below its liquid–liquid critical temperature. We report here simulations along a subcritical isotherm, for which two liquid states with the same pressure and temperature but different density can be equilibrated. This allows for a clear visualization of the structural changes taking place across the transition. We specifically focus on how the topological properties of the H-bond network change across the liquid–liquid transition. Our results demonstrate that the structure of the high-density liquid, characterized by the existence of interstitial molecules and commonly explained in terms of the collapse of the second neighbor shell, actually originates from the folding back of long rings, bringing pairs of molecules separated by several hydrogen-bonds close by in space.





## I. INTRODUCTION

The experimental evidence supporting the possibility of a liquid–liquid critical point (LLCP) in supercooled water is constantly growing.[1–7] From the 1992 seminal study by Poole *et al.*,[8] several models,[9–12] including recently a quantum-based machine-learning potential,[13] have been scrutinized to support the idea that water, despite being a pure molecular liquid, in deep supercooled states can exist in two different liquid forms. Until recently and despite a significant collective effort, definitive numerical evidence based on the analysis of the density fluctuations close to the liquid–liquid critical point and finite size scaling was available only for the ST2 model,[14–17] a model known to overemphasize tetrahedrality in the local structure. Only last year, a numerical tour-de-force investigation[18] finally provided conclusive evidence that two of the most realistic classical models for water[19] (TIP4P/2005[20] and TIP4P/Ice[21]) do show a clear liquid–liquid critical point in deep supercooled states. This study, together with the previously cited recent outstanding experiments,[1–6] strongly supports the possibility that not only the models but also real water exists in two distinct liquid forms. Recent reviews[22–26] provide a detailed description of the interesting behavior of supercooled and glassy water.

The availability of a realistic model that can be numerically studied even below the liquid–liquid critical point, although with a significant computational effort, offers the unprecedented possibility to identify the structural units driving the first-order transition, thus deciphering the microscopic mechanisms at the origin of the LLCP in water.

In this paper, we extend previous simulations and investigate novel state points, covering the range from $P = 1$ bar to $P = 4000$ bars at $T = 188$ K for a system of $N = 1000$ molecules interacting via the TIP4P/Ice potential. In this model, the liquid–liquid critical point is found at $T_c = 188.6$ K, $\rho_c = 1.015$ g/cm$^3$, and $P_c = 1725$ bars.[18] The possibility to compare the low and high density liquids (LDL and HDL) at the same $P$ and $T$ in metastable equilibrium offers a vivid representation of the structural changes taking place at the transition. We find that both low and high density liquids are essentially fully bonded, meaning that all hydrogens (>99.9%) are engaged in hydrogen bonds with close-by oxygen atoms. The fraction of molecules with four bonds, in the classic two-donor two-acceptor geometry, is larger than 95%. Increasing the density across the transition, the tetrahedral geometry is distorted, opening the possibility of novel HB patterns, as highlighted by the changes in the statistics of ring-loops and their spatial geometry. We discover that the presence of interstitial molecules at relative distances of 0.35 nm, previously assumed to arise from the collapse of the second shell, originates from the folding back of long rings, bringing molecules separated by paths of several hydrogen bonds at close distances.

Thus, pairs of molecules close by in space (≈0.35 nm) are seeds of two distinct networks, facing each other, which merge together after three or four bonds due to the disorder of the network. Introducing a combined structural and topological analysis, we show that unambiguous differences in the HB network properties exist between the two liquids.

## II. NUMERICAL METHODS

MD simulations were performed in supercooled conditions on the TIP4P/Ice water model[21] using GROMACS 5.1.4,[27] in the NPT ensemble. All simulations were run with a leap-frog integrator with a time step of 2 fs, and temperature coupling was controlled via the Nosé–Hoover thermostat with a characteristic time of 8 ps, and pressure coupling was controlled via an isotropic Parrinello–Rahman barostat with a characteristic timescale of 18 ps. In all cases, a cubic simulation box with periodic boundary conditions was adopted, and each simulation was initialized from a different initial configuration. Molecular constraints were implemented with the LINCS algorithm at the sixth order. van der Waals interactions have been evaluated with a cutoff distance of 0.9 nm, and this same cutoff distance was adopted for the real-space cutoff of electrostatic interactions evaluated by the particle-mesh Ewald method at the fourth order. We explored the $T = 188$ K isotherm in a system of $N = 1000$ molecules, with pressures ranging from 1 bar to 4000 bars.

If not stated otherwise, all results shown throughout this work are evaluated on the inherent structures (IS).[28,29] The inherent structure of a system can be operationally defined as the local energy minimum that is reached via a (constant volume) steepest descent path starting from an equilibrated configuration. In this process, all vibrational degrees of freedom are brought to their ground state. To numerically evaluate the IS, we used the double-precision version of the steepest descent algorithm in GROMACS with a force tolerance of 1 J/mol/nm and a maximum step size of $5 \times 10^{-4}$ nm. Details on simulation and equilibration times for each state point can be found in Table S1 of the supplementary material.

## III. RESULTS: STRUCTURAL AND THERMODYNAMIC QUANTITIES

### A. Thermodynamic quantities

Figure 1(a) shows the time evolution of the density at $T = 188$ K for different values of $P$. Close to the liquid–liquid transition ($P = 1800$ and $P = 1900$ bars), two independent simulations have been performed, starting from opposite sides of the transition line. At $P = 1900$ bars, after 5 $\mu$s, we observe a transition from low to high density. At $P = 1800$ bars, no crossing is observed in 25 $\mu$s of the simulation, providing two trajectories with the same pressure and temperature but different densities, as expected close to a coexistence line and, more importantly for us, two simulations that can be scrutinized to highlight the differences between the low and high density liquids, at the same $P$ and $T$.

The equation of state at $T = 188$ K is shown in Fig. 1(b). Consistent with the first-order nature of the transition, the density discontinuously jumps from ≈0.95 to ≈1.05 g/cm$^3$. A discontinuous jump of ≈1 kJ/mol is also observed in the pressure dependence of the energy (per molecule) of the inherent structures, reported in

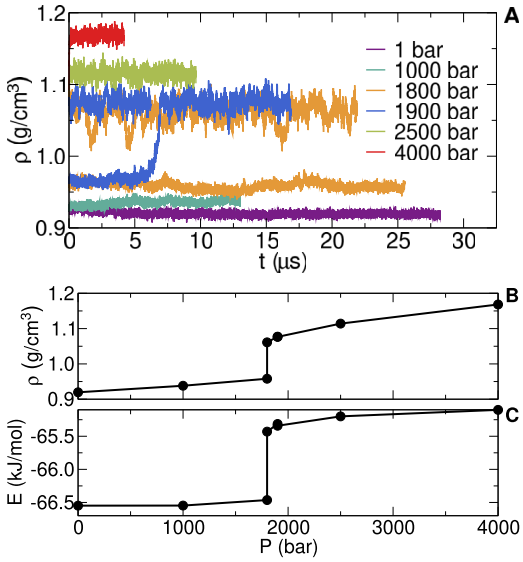


**FIG. 1.** Thermodynamic behavior along the $T = 188$ K isotherm. (a) Fluctuations in the density during the numerical simulations. (b) Equation of state and (c) potential energy per molecule evaluated in the IS. We point out that the amplitude of the jump in energy observed in the IS is identical to that in the real dynamics.

Fig. 1(c). The condition of thermodynamic coexistence also requires, besides equality of $T$ and $P$, the equality of the chemical potential (Gibbs free energy per particle). Hence, from the changes in $\Delta\rho$ and $\Delta E$ at the transition, it is also possible to estimate the change in the entropy per molecule $\Delta S$ from

$$\Delta\mu = \Delta E + P\Delta V - T\Delta S = 0. \quad (1)$$

From the low density to the high density state at $T = 188$ K and $P = 1800$ bars, we observe $\Delta E \approx 1$ kJ mol$^{-1}$ and $\Delta V \approx -2.7$ Å$^3$ per molecule, which result in $\Delta S \approx 3.7$ J mol$^{-1}$ K$^{-1}$. The high-density liquid is thus more disordered than the low-density one, even though it is denser. Experimental investigations on the corresponding low density and high density amorphous states (LDA and HDA)[30] report a smaller value, $\Delta S \approx 1$ J mol$^{-1}$ K$^{-1}$. In the two-state model framework,[31] entropy differences between pure LDL and HDL for ST2 and TIP5P water have been estimated, respectively, as ≈ 2.5 and ≈3 J mol$^{-1}$ K$^{-1}$ on real configurations. The slope of the coexistence curve at this state point is $dP/dT|_{coex} = \Delta S/\Delta V \approx -23$ bars K$^{-1}$.

### B. Hydrogen bond

The ability to provide a proper definition of hydrogen bond (HB) between two molecules is crucial for any analysis of the hydrogen bond network in water. Usually, librational and vibrational distortions complicate the HB definition, but their effect can be subtracted by a potential energy minimization.[32] Figure 2 shows for each pair of molecules the relative oxygen–oxygen distance $r$ and the angle $\theta$, defined as the smallest among the four HÔO angles (the angles between the intramolecular OH bond and the intermolecular OO line). Figures 2(b) and 2(c) show very clearly that at this low $T$, after minimization, there is a well-separated island of points centered at

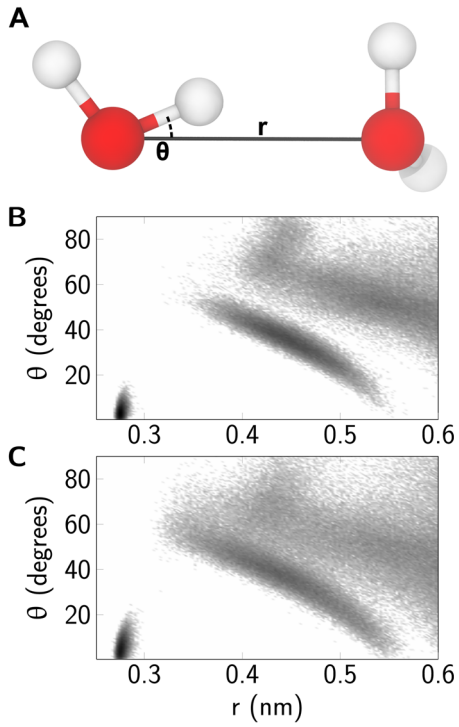


**FIG. 2**. (a) Cartoon representation of intermolecular O–O distance $r$ and minimum HÔO angle $\theta$ used for HB identification. Values of $r$ and $\theta$ have been collected (in the IS) between each pair of water molecules to evaluate the joint orientation–distance distribution $P(r, \theta)$. Points were sampled from NPT simulations at $T$ = 188 K and $P$ = 1800 bars, in (b) low and (c) high density states. Probability density $P(r, \theta)$ is represented by color intensity (increasing from white to black) in log scale.

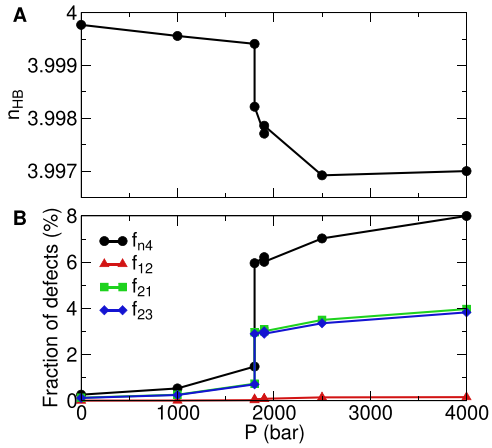


**FIG. 3**. Pressure dependence of (a) the average number of HBs per molecule and (b) the fraction of the different species of coordination defects. $f_{nm}$ is the fraction of $H^nO^m$ molecules, and $f_{n4} = f_{12} + f_{21} + f_{23}$.

$r \approx 0.28$ nm with $\theta < 30°$; this region can be unambiguously associated with hydrogen bonds. In agreement with the geometric criterion of Luzar and Chandler,[33] from now on, we will define two particles to be H-bonded if $r < 0.35$ nm and $\theta < 30°$ (in the inherent structure configuration). The more elongated island with $\theta < 60°$ and $r < 0.55$ nm in the low density state arises from the second shell of neighbors; in the high density state, this island expands toward lower values of $r$ with increasing $\theta$ so that the net separation between the shells decreases. At the same time, it overlaps substantially with the outer one, hinting at a significant spatial mixing between distinct neighbor shells. More complete analysis of the joint orientation-distance distributions in water can be found elsewhere.[34–36]

In the supplementary material (Figs. S1–S3), the main results of our analysis are reproduced on the real structures of the system. It is shown that our structural description retains its validity even in the real dynamics, i.e., in the presence of thermal distortion.

The possibility to define the existing HBs unambiguously makes the analysis of the HB network quite revealing. Figure 3(a) shows that at this temperature, essentially all hydrogens are involved in HBs, at all values of $P$. The average number of HBs per particle $n_{HB}$ is always larger than 3.99. At ambient pressure, it reaches the value $n_{HB} = 3.9997$, an almost perfect tetrahedral network. Correspondingly, the fraction of H atoms that do not participate in any bond, $1 - n_{HB}/4$ (assuming that no H atom can participate in more than 1 HB), is $\approx 7.5 \times 10^{-5}$ in LDL and $\approx 7.5 \times 10^{-4}$ in HDL. The network has reached essentially a fully bonded state, in both the low and the high density liquid phases.

Despite practically all H being involved in one HB, not all molecules show a tetrahedral coordination. All molecules whose bonding pattern deviates from the ideal two donated bonds plus two accepted bonds can be regarded as network defects. The idea that water could be described as a defective network of HBs, in which bonds break and reform on a quite fast timescale (ps at ambient temperature) providing fluidity to the material, is not new.[37–40] The defects have also been associated with molecular mobility,[41–44] being the network restructuring more efficient in the presence of such defects acting as catalyzers for bond swaps. In particular, the swap mechanism has been characterized quite precisely in the case of the nearby presence of one over- and one under-coordinated molecule.[43] Their structural role and a possible connection with the liquid–liquid phase transition have not been clarified yet.

The defects observed in the explored thermodynamic range are three- and five-coordinated molecules. The three-coordinated molecules coincide with the "$D$" molecules in Ref. 45. Following the notation of Saito *et al.*,[44] these molecules will be identified, respectively, as $H^2O^3$, $H^1O^2$, and $H^2O^1$, where $H^nO^m$ means that the H atoms donate $n$ bonds and the O atom accepts $m$ bonds. Figure 3(b) shows the $P$ dependence of the fraction of different species $f_{nm}$ and their sum (the fraction of non-four-coordinated molecules $f_{n4}$). In the low density liquid, $f_{n4}$ is less than 1%, all H are bonded ($f_{12} \approx 0$), and $f_{21} = f_{23}$. The low density liquid can thus be represented as a fully bonded tetrahedral network, with excitations composed of $H^2O^1$–$H^2O^3$ pairs, preserving the total number of bonds. In the high density liquid, $f_{n4}$ is roughly 8%, with $f_{21}$ only slightly smaller than $f_{23}$ and a fraction $f_{12}$ smaller than 0.15% of un-bonded hydrogens. Hence, even the high density liquid has a large majority (>92%) of tetrahedrally coordinated molecules. At the transition, the number of non-tetrahedral coordinated molecules jumps from ≈2% to ≈6%. We never observe $H^3O^2$ molecules, in which the same proton binds to two different oxygens.[46] In the study of Saito *et al.*,[44]

which focuses on network defects on a wider thermodynamic range, no mention of $H^3O^2$ has been made; other works using the "bifurcated bond" nomenclature[41,43] do not distinguish explicitly between $H^2O^3$ and $H^3O^2$.

We note on passing that, as we have alluded previously, $H^1O^2$ describes an un-bonded proton, a geometry that sacrifices one HB and whose probability becomes smaller and smaller on cooling. It has been suggested[44] that the $H^1O^2$ defects play a more central role as a promoter of structural changes, facilitating rotational and translational motions in water. Hence, despite vanishingly rare, they could retain some fundamental role in the glassy dynamics of water and explain the higher mobility of the high density liquid compared to the low density one. The almost perfect matching of $f_{23}$ and $f_{21}$ at this extremely low temperature also suggests that possibly these network defects are created in pairs and, once created, propagate in the network. Finally, we also note that in the low density phase at atmospheric pressure, configurations with no defects (out of 1000 molecules) are sampled during the course of the simulation, providing, to our knowledge, the first *brute force* generation of a perfect random tetrahedral network in water.

Figure 4 shows the distribution of the potential energy per molecule in the IS at $P = 1800$ bars for both the low and the high density liquid, separating the contributions from molecules with different coordination numbers. It is apparent from the data that five (three-)-coordinated molecules have a lower (higher) energy compared to the four-coordinated molecule, supporting the view that the combined creation of $H^2O^1$ and $H^2O^3$ has a relatively small energetic cost since it does not require a change in the total number of hydrogen bonds. We also note that there is a net effect of the density on the tetrahedrally coordinated molecules ($H^2O^2$): as the density increases, their energy distribution displays an increase in variance toward the high-energy side. The average energy variation per molecule from LDL to HDL is $\Delta E \approx 1$ kJ mol$^{-1}$; the separate contributions based on the coordination number are $\Delta E_4 \simeq 0.95$, $\Delta E_3 \simeq -0.96$, and $\Delta E_5 \simeq 0.46$ kJ mol$^{-1}$. Three-coordinated molecules are favored in the HDL state, while five-coordinated molecules are favored in the LDL state. Assuming for convenience that defects are created *exactly* in pairs in both states, defining the average energy of a defect $(E_3 + E_5)/2 \equiv E_{n4}$, and denoting the HDL and LDL states with superscripts H and L, respectively,

$$\begin{aligned}\Delta E = E^{H} - E^{L} &= \left(1 - f_{n4}^{L}\right)\Delta E_4 + f_{n4}^{L}\Delta E_{n4} \\ &\quad + \Delta f_{n4} E_{n4}^{L} - \Delta f_{n4} E_4^{L} \\ &\quad + \Delta f_{n4}\left(\Delta E_{n4} - \Delta E_4\right) \\ &= \Delta E_{\rho} + \Delta E_{def} + \Delta E_{c}.\end{aligned}$$

Three distinct contributions to the energy variation are identified: density increase (and hence network distortion), creation of defect pairs, and a coupling term. Extracting the relevant quantities from the MD trajectories, one obtains $\Delta E_{n4} \approx -0.25$ kJ mol$^{-1}$, $E_4^L \approx -66.8$ kJ mol$^{-1}$, $E_{n4}^L \approx -63.5$ kJ mol$^{-1}$, and $f_{n4}^L \approx 1.5\%$, $\Delta f_{n4} \approx 4.5\%$; therefore, the three contributions are $\Delta E_\rho \approx 0.93$, $\Delta E_{def} \approx 0.15$, and $\Delta E_c \approx -0.05$ kJ mol$^{-1}$. The two components of the defect contribution are large but mostly cancel each other out since the energy of a 3–5 defect pair is only slightly higher than that of a tetrahedral pair. The dominant effect of the density increase is a distortion of the HB network structure; even though defects gain some stability from the network distortion ($\Delta E_{n4} < 0$), their concentration is too low to counterbalance the energy increase in the distortion of the tetrahedrally coordinated molecules.

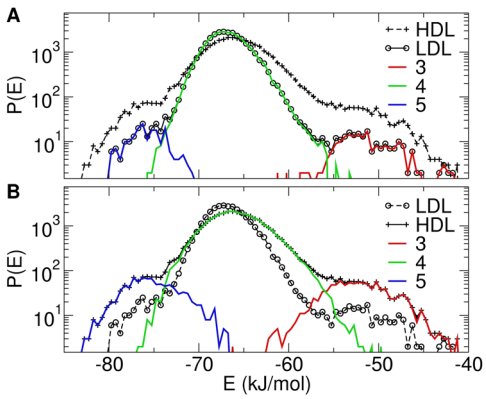


**FIG. 4.** Distribution of potential energy per molecule in the inherent structures at $T = 188$ K and $P = 1800$ bars. Each of the two panels shows the contribution from both LDL and HDL for better comparison. In (a), the separation in the contributions from three-, four-, and five-coordinated molecules is referred to the LDL; in (b), it is referred to the HDL.

## C. Structural quantities

X-ray scattering experiments yield a description of the molecular structure of water in terms of the oxygen–oxygen structure factor $S(q)$, the Fourier transform of density fluctuations in the system.[47] Figure 5(a) shows the O–O structure factor in the two coexisting liquids at 1800 bars (evaluated in the IS). The two states display distinct first diffraction peaks at $q \approx 17$ and $\approx 21$ nm$^{-1}$, respectively.[6,48] The O–O radial distribution function $g(r)$ for the low and high density liquid is shown in Fig. 5(b). Having subtracted the vibrational and librational components, both states show $g(r) \approx 0$ at $r \approx 0.31$ nm, an indication of a very well-defined first coordination shell. For $r > 0.3$ nm, clear differences emerge between the two liquids: the high density liquid displays a significant presence of interstitial molecules between the first and second coordination shells, while the low density liquid has a well-defined second peak at a distance of $\approx 0.44$ nm, consistent with a tetrahedral bonding geometry. A large number of studies, both numerical and experimental, have focused on understanding the characteristic features of distinct structures of liquid water. It is now acknowledged that the main difference between the LDL and the HDL lies in the region between the first two minima of oxygen–oxygen $g(r)$, i.e., the second shell;[49,50] in particular, while the second shell of the low-density structure is consistent with an optimal tetrahedral arrangement, the second shell of the high-density one is observed to "collapse" toward the first.[51]

The full pressure dependence of $S(q)$ and $g(r)$ at $T = 188$ K is reported in Figs. S4 and S5 of the supplementary material, for both inherent and real structures. A significant growth upon compression is observed in $g(r)$ at the interstitial separation ($r \approx 0.35$ nm), while the tetrahedral peak ($r \approx 0.44$ nm) weakens. These results are consistent with the experimentally determined structures of the amorphous phases of water.[52,53] The trend

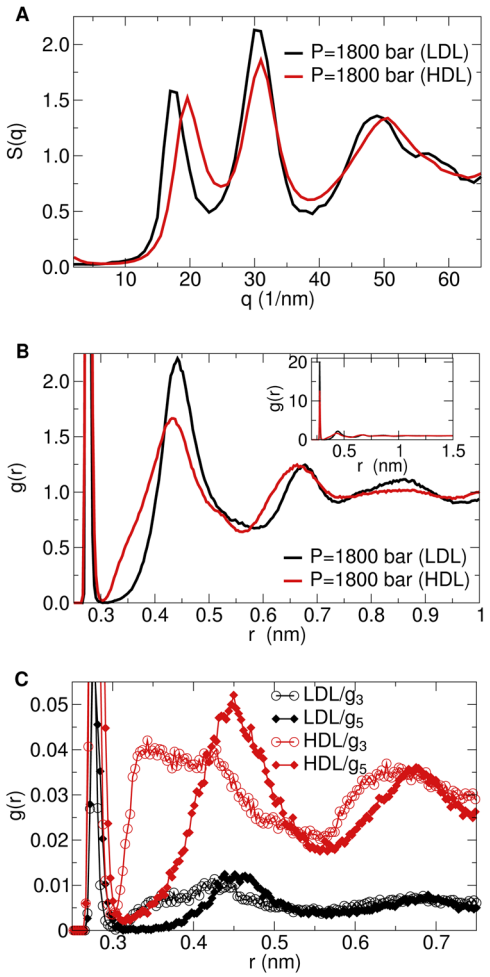


**FIG. 5**. Structural differences between the LDL and HDL states at $T$ = 188 K and $P$ = 1800 bars in the inherent structures. (a) Oxygen–oxygen structure factor and (b) radial distribution function in the two coexisting liquid states. (c) Contribution of the defects to $g(r)$ in the two states.

displayed by the first diffraction peak, which continuously shifts to higher values as $P$ is increased, is also consistent with the transformation of HDA to VHDA. We note on passing that the HDL structure reported in Figs. 5(a) and 5(b) displays only a small deviation from tetrahedrality (compared to the one observed at larger pressures) since the system is close to the critical point and the structural differences between the two coexisting liquid phases are not very pronounced.

To estimate the effect of network defects on the average structural quantities, we evaluate $g_3$ and $g_5$, $g(r)$ evaluated around a reference molecule with three and five HBs, respectively. Both $g_3$ and $g_5$ are normalized such that the large $r$ limit coincides with their relative concentration to highlight their relevance in total $g(r)$. Figure 5(c) shows that the local environment of three-coordinated molecules is significantly populated at $r \approx 0.35$ nm in both LDL and HDL states. Although it is much weaker, five-coordinated molecules also show some tendency to populate the interstitial region, but only in the HDL. However, Fig. 5(c) shows that due to their small concentration, coordination defects' net contribution to $g(r)$ is practically irrelevant: their presence cannot explain, alone, the presence of interstitial molecules in HDL. The vast majority of interstitial molecules must thus be tetrahedrally coordinated molecules surrounding other tetrahedrally coordinated molecules.

## IV. RESULTS: RINGS AND NETWORK TOPOLOGY

### A. Particle-rings

The possibility to define unambiguously the hydrogen bonded pairs at the explored temperatures (Fig. 2) offers the possibility to investigate the topology of the HB network and its changes across the LL transition. We will consider the HB network as undirected, and our investigation will make use of two basic concepts. The first is the chemical distance $D$ between two molecules, defined as the length of the shortest HB path connecting them; the set of molecules at the same chemical distance $D$ from a central molecule is said to constitute its $D$th *bond-coordination shell*, which is to be distinguished from the notion of the coordination shell as identified by the minima of $g(r)$. The second concept is that of ring, which we define as a closed path along the HB network, whose total length $L$ is measured in units of chemical distance.

The analysis of the ring statistics is not new in the structural studies of network-forming materials, and many different non-equivalent definitions of "ring" (or loop) have been proposed throughout the last 50 years, providing sometimes contrasting physical interpretations.[54–58] We adopt a definition that relies on the length of the shortest path between two molecules, without considering the donor/acceptor property of each bond, in favor of both simplicity and robustness.

To provide a characterization of the local bonding environment around a given molecule $i$, we evaluate, for each pair ($j$, $k$) of first-bonded neighbors of $i$ (i.e., at chemical distance one), the shortest closed path, starting and ending in $i$, which contains both $j$ and $k$. This closed path will be called a *particle-ring* of molecule $i$. This is equivalent to summing the two shortest non-intersecting paths starting at $j$ and ending at $k$ (one of which is always the path $j - i - k$). The length of the particle-ring is evaluated in units of chemical distance. Using this definition, a tetrahedrally coordinated molecule has exactly six particle-ring lengths associated with it. Instead, a three (five) coordinated molecule has three (ten) particle-ring lengths.

In a crystalline ice $I_h$ configuration, all six particle-rings emanating from a generic molecule have a length of 6. The disorder of the liquid phase manifests in the existence of a continuum of local molecular environments, resulting in a distribution of particle-ring lengths. Figure 6(a) shows the fraction $P(n_6)$ of tetrahedral molecules with a given number $n_6$ of hexagonal particle-rings in the two liquid states. The HDL has on average ≈2.5 hexagonal particle-rings, while the LDL has on average ≈3.5 of them.

Particularly interesting is the distribution of particle-ring lengths in the low- and high-density liquid at $P$ = 1800 bars, shown in Fig. 6(b). The LDL has a larger population of hexagonal particle-rings and a smaller fraction of five- and seven-membered ones (with negligible concentrations of $L$ = 4 and $L$ = 8). The HDL is instead characterized by a more disordered particle-ring distribution, with a non-negligible presence of particle-rings of lengths 4 and 8 and a

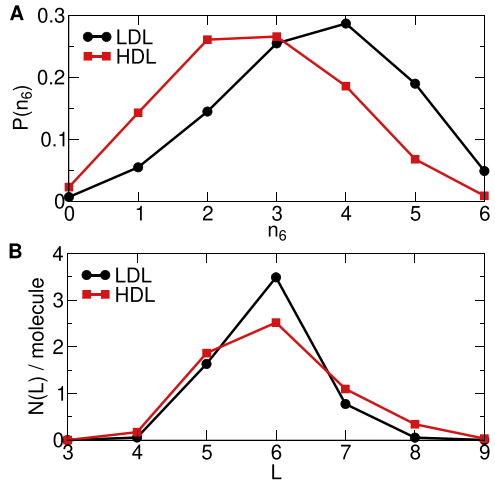


**FIG. 6**. Particle-ring statistics in the LDL and HDL state at $T$ = 188 K and $P$ = 1800 bars. (a) Fraction of tetrahedrally coordinated molecules with $n_6$ hexagonal rings steaming out from their four bonds ($0 \le n_6 \le 6$). (b) Distribution of particle-ring lengths, normalized to represent the average number of rings of a given length per molecule.

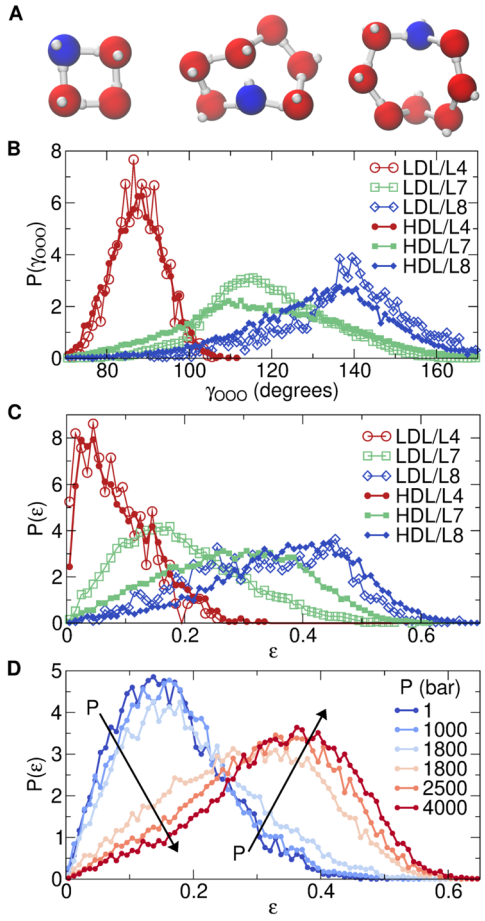


**FIG. 7**. Geometric properties of particle-rings. (a) Cartoon representation of particle-rings of lengths 4, 7, and 8 with the seed molecule highlighted in blue. (b) Distribution of the O–O–O angles of particle-ring seeds and (c) of the elongation factor of particle-rings in the LDL and HDL states at $T$ = 188 K and $P$ = 1800 bars. (d) $P(\varepsilon)$ in particle-rings of length 7 along the 188 K isotherm shows a clear bimodal nature. All curves are normalized, thus the underlying areas do not reflect the concentration of each population.

few of length 9. Thus, particle-rings of lengths 4 and 8 could act as possible indicators of typical HDL local environments.

Representative images of particle-rings of various lengths are shown in Fig. 7(a). To quantify the variability in their morphological properties, we evaluate two geometric quantities: the O–O–O angle of the seed molecule, $\gamma_{OOO}$, and the elongation factor of the ring $\varepsilon = (I_2 - I_1)/I_3$, where $I_n$ is the $n$th eigenvalue of the ring inertia tensor (sorted by increasing magnitude).[59] $\varepsilon$ has values between 0 for a radially symmetric arrangement and 1 for a linear arrangement. The results are shown in Figs. 7(b) and 7(c) for four-, seven-, and eight-membered particle-rings.

Tetragonal rings have a peculiar and well-defined shape, for which only two types of arrangements have been identified in our simulations: i) each molecule donates and accepts one HB (in-ring); ii) two molecules donate one and accept one HB, one molecule donates two HBs, and one molecule accepts two HBs. The morphology of these particle-rings is identical in both liquid states, suggesting that they are not affected by the transition. Heptagonal particle-rings are significantly present in both LDL and HDL (Fig. 6) and show a very broad $\gamma_{OOO}$ distribution, hinting at the fact that there is no strict geometric constraint on their formation and they can adapt to various shapes. This is also confirmed by their $P(\varepsilon)$, showing that they can range from "circular" configurations to folded and elongated ones. Octagonal particle-rings have seeds with large characteristic $\gamma_{OOO}$ angles, sometimes reaching configurations with almost-collinear triplets of oxygens, although their distribution is broad and rings with tighter angles are also found. Their distributions do not undergo a drastic change across the transition, but, while they clearly favor elongated configurations, they can still adopt a variety of morphologies, as implied by the long tails of $P(\varepsilon)$. Seven-membered particle-rings are the ones to undergo the most drastic morphological transformation across the transition; the full pressure dependence of their $P(\varepsilon)$ is drawn in Fig. 7(d), showing a distinct bimodal nature. While their concentration increases only slightly with increasing density, most of them deform to take on elongated shapes so that the HDL is dominated by elongated rings: the average elongation of seven-membered particle-rings goes from ≈0.16 at ambient pressure up to ≈0.34 at 4000 bars. All the other particle-rings (except tetragonal) show a similar tendency to increase $\epsilon$, but not as clear and pronounced.

## B. Merging structure and network properties

It is well known that the second coordination shell, i.e., the spherical shell formed by neighbors at a distance between the first and second minima of the radial distribution function from the central atom, is crucial for a structural description of liquid water.[49–51] In the case of network-forming liquids, we find particularly informative to distinguish between *shells* in real space distance, as commonly

defined by the minima of the $g(r)$,[60] and *bond-coordination shells*, as indicated by the chemical distance. This network-inspired separation of the different contributions of the radial distribution function provides a novel unexpected result: the main contribution to the collapse of the second shell observed in real space, which is associated with the LL transition, actually originates from the "folding" of rings longer than 6, which brings pairs of topologically distant molecules, in particular those at chemical distances 3 and 4, at short distances in space.

To quantify this observation, we start by evaluating the contribution of each distinct bond-coordination shell to $g(r)$ so that $g(r) = \sum_D g_D(r)$, where $g_D(r)$ is the radial distribution function evaluated among only pairs of molecules at chemical distance $D$. A sample result of this procedure, applied in the low density state at 1800 bars, is shown in Fig. 8(a). One should notice that *peaks in $g(r)$ do not directly mirror peaks in the underlying $g_D$ contributions*. Related to the interstitial molecule phenomenon ($r \approx 0.35$ nm) are the distributions for chemical distances $2 \le D \le 4$, shown in Fig. 8(b) in both LDL and HDL at the same $P$. The increase in density couples with the broadening of all coordination shells and, interestingly, to the significant growth of a population in the third and fourth bond-coordination shell at distances corresponding to the second spatial shell. These changes become even more clear if the full pressure dependence of $g_D$ along the $T = 188$ K isotherm is examined, as shown in Fig. 8(c), for each of these bond-coordination shells. Upon increasing $P$, the second bond-coordination shell significantly broadens, populating both distances smaller and larger than the typical tetrahedral geometry, with a net shift toward lower separation values. However, the most striking result is the growth in the HDL of well-defined peaks in the interstitial region (≈0.35 nm) arising from molecules at chemical distances $D = 3$ and $D = 4$. These peaks are thus an intrinsic feature of the high density liquid and a clear evidence of a structural change in the network topology across the LDL-HDL transition.

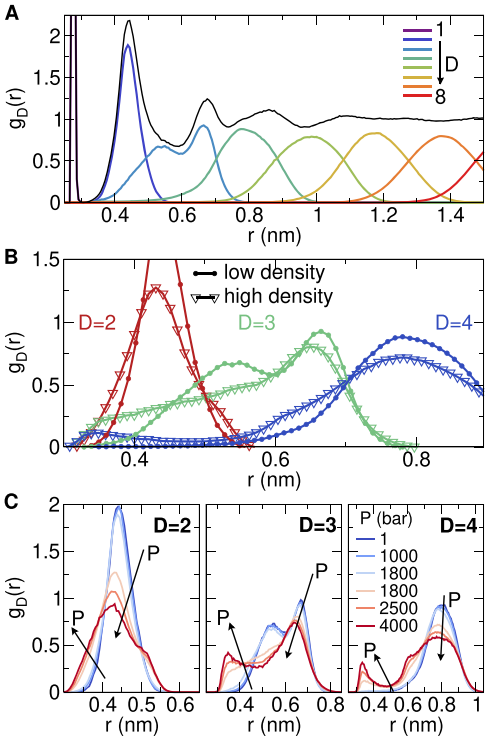


**FIG. 8.** (a) $g(r)$ of water (black) splitted in the contributions arising from each distinct bond-coordination shell from $D = 1$ to $D = 8$ in LDL at $P = 1800$ bars. (b) Close-up view on the $g(r)$ contributions from second to fourth bond-coordination shells. Curves have been evaluated from simulations at $T = 188$ K and $P = 1800$ bars, in the low and high density states. Colors are matched per bond-coordination shell. (c) Pressure dependence of the $g(r)$ contributions from second, third, and fourth bond-coordination shell along the 188 K isotherm.

A closer look at the details of this topological transformation is obtained by further separating the radial distributions $g_D$ in the contributions arising from different ring lengths. Here, for each pair of molecules at chemical distance $D$, we evaluate the length of the two shortest non-intersecting paths connecting the two molecules and define the ring length $L$ as the sum of these two lengths. This definition of *ring* is not to be confused with that of the particle-ring given previously since no central particle is involved (although rings associated with particles with $D = 2$ do coincide with particle rings for any ring length $L$). We then separate each $g_D(r)$ into the contributions from each ring population $g_D(r) = \sum_L g_D^L(r)$. By definition, the minimum ring length between two molecules at chemical distance $D$ will satisfy $L \ge 2D$.

The resulting radial distribution function $g_D^L$, evaluated on the LDL and HDL states at 188 K and 1800 bars, is shown in Fig. 9. Our discussion will start from the second bond-coordination shell [Figs. 9(a) and 9(d)]. As we move from LDL to HDL, we observe, along with a drastic decrease in the population of hexagonal rings (expected, and already evident from Fig. 6), a broadening in the contribution of heptagonal rings, a symptom of the increased disorder. What is probably most interesting is, however, the presence of tetragonal and octagonal rings in the HDL, which are nearly absent in the LDL. Tetragonal rings are distorted "square" configurations whose diagonals contribute to the peak around ≈0.38 nm, implying that the O–O–O angles between each triplet of adjacent molecules lie around an average of ≈87°. Pairs at $D = 2$ in octagonal rings show instead a clear peak at distances ≈0.52 nm, indicating almost-collinear triplets of H-bonded molecules, a highly distorted arrangement.

In the third bond-coordination shell [Figs. 9(b) and 9(e)], the population of hexagonal rings diminishes but develops a fatter low-$r$ tail, and a major distortion in both heptagonal and octagonal structures is observed, populating the interstitial region; longer rings also show extending tails, but their contribution in the region of the second spatial shell is negligible.

The situation in the fourth bond-coordination shell [Figs. 9(c) and 9(f)] is particularly revealing. Both octagonal and enneagonal rings grow a secondary peak centered around $r \approx 0.35$ nm in HDL. Larger rings develop long tails but contribute only negligibly to the second spatial shell. The peaks from eight- and nine-membered rings provide a contribution in the interstitial region that is completely missing in the LDL phase; this can only happen if these rings fold back on themselves so that topologically distant pairs of molecules on the opposite sides of the ring are brought close to each other.

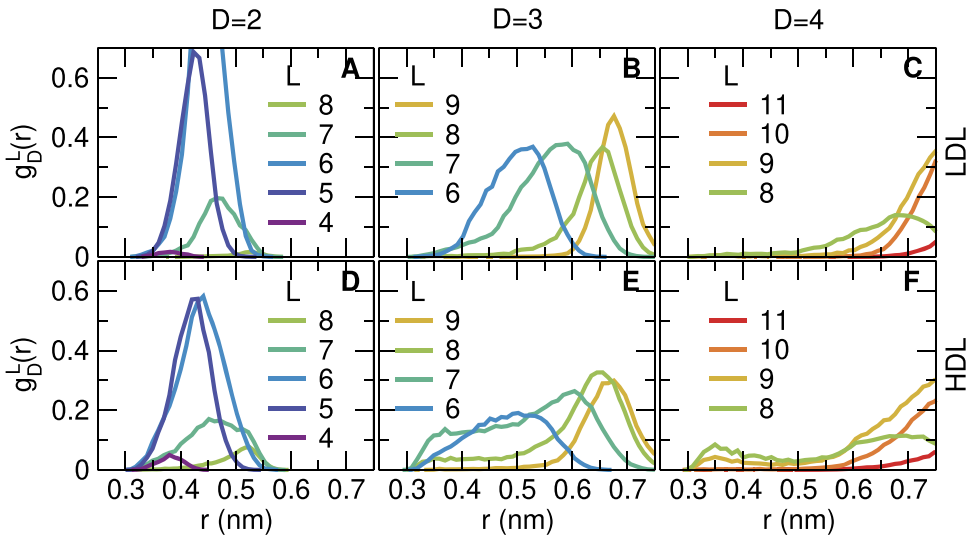


**FIG. 9**. Contributions to oxygen–oxygen $g(r)$ of water separated by chemical distance $D$ and ring length $L$ in the low-density (a)–(c) and high-density (d)–(f) states at $P$ = 1800 bars and $T$ = 188 K. Of particular interest are the clear peaks for $D$ = 4 in the interstitial region of the high density liquid (f).

To better clarify the methodology, we show in Fig. 10 a collection of rings, characteristic of the HDL state, with their classification in terms of chemical distance $D$ and minimum ring length $L$. The two blue molecules are the ones for which the distance in real space $r$ is calculated.

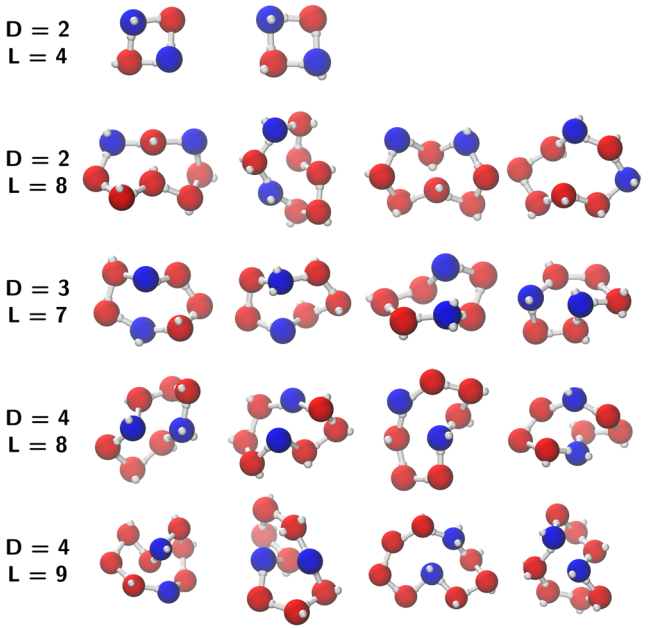


**FIG. 10**. Representative images of different types of rings highlighting some of the structural features of the high-density liquid. The blue molecules are the ones between which the distance $r$ is calculated. The D2L4 structures are more square-like if all four participating molecules donate at most one HB and more rhomboid if one of the molecules donates two HBs, imposing a tetrahedral angle. The D2L8 rings have been chosen such that $r > 0.5$ nm to highlight the highly distorted, quite collinear, elongated bonds. All the other examples (D3L7, D4L8, and D4L9) have $r < 0.37$ nm so that each blue molecule is an interstitial molecule for the other one.

To highlight these important changes in the topology of the HB network, we show the pressure dependence of the four most interesting contributions in Fig. 11 from ambient pressure up to 4000 bars, clearly indicating the onset of peaks in these distributions in the HDL phase, hence hinting at a potential definition for a local order parameter of the LDL–HDL transition. In particular, the signal from D2L8 rings [Fig. 11(b)] is essentially zero in LDL and significantly different from zero in HDL; so is the signal from D3L7 and D4L8 rings [Figs. 11(c) and 11(d)] in the regions $r < 0.45$ nm and $r < 0.5$ nm, respectively, with the latter showing a much more polished peak. Tetragonal (D2L4) rings [Fig. 11(a)] also show a similar two-state behavior, but they are not completely absent in the LDL. Interestingly, there is no significant pressure-induced change in the shape of their distribution within each phase. A connection between the presence of tetragonal rings and interstitial molecules was already hypothesized, but not fully developed, by Svishchev and Kusalik.[34] However, their concentration is quite small, so they provide only a minor contribution to $g(r)$, comparable to that of network defects [Fig. 5(c)].

The existence of pairs of molecules lying at intermediate distances between the first and second peaks of $g(r)$ as a result of the formation of long folded rings is thus a structural signature of the HDL.

Figure 12 offers a visual representation of the local network structures around close-by ($r < 0.37$ nm) pairs of molecules at $D$ = 4 in eight-membered rings, which are arguably the most significant feature of the HDL. The two reference molecules can be considered as the seeds of two tetrahedral networks, which retain their independence up to the second generation. These configurations show different aspects of the high density structures. In the left panel, the ring has a re-entrant cusp-like apex so that the two molecules can get close to each other by interpenetrating their networks (although only on a short length scale); while clearly limited in space by disorder, this type of interpenetration might be reminiscent of the "full" network interpenetration observed in the crystalline phases of ices VI and VII. In the middle panel, the ring displays a folded and strongly non-planar structure so that molecules on

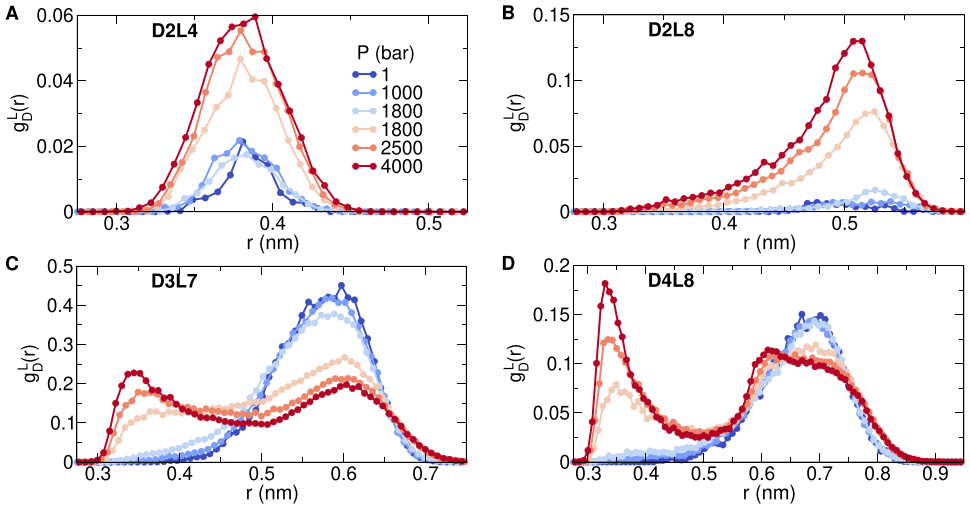


FIG. 11. Close-up view on the pressure dependence of the $g(r)$ contributions from (a) D2L4, (b) D2L8, (c) D3L7, and (d) D4L8 rings along the 188 K isotherm. Legend shared among all panels. Salient characteristics of these distributions are the clear distinctive peaks arising from D3L7 and D4L8 rings in the interstitial region of the HDL; furthermore, D2L8 rings are essentially a unique feature of the high-density phase.

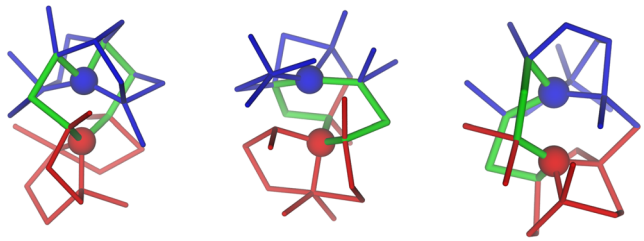

FIG. 12. Networks departing from two close-by molecules at chemical distance $D = 4$ in a ring of length $L = 8$. The two reference molecules are identified by blue and red spheres and are at distances $r < 0.37$ nm; each molecule's HB network up to the second generation is represented by blue and red sticks, respectively. The ring is identified by green sticks. Configurations sampled from simulation data in the HDL at $P = 1800$ bars.

opposite sides of the ring end up close together; in this case, the networks appear to grow in opposite directions, as if repelling each other. A similar repulsive effect is seen, perhaps even more vividly, in the right panel; this network repulsion could be suggestively compared to the structural distortions that the HBs undergo when facing a hydrophobic surface. We also note that the eight-membered ring connecting the two molecules can be degenerate.

## V. CONCLUSIONS

We have provided a quantitative description of the structural changes taking place at the liquid–liquid transition in the TIP4P/Ice model, a model for which the existence of a genuine second order phase transition, characterized by fluctuations consistent with the Ising universality class in three dimensions, has been recently demonstrated.[18] We have focused on an isotherm below the critical temperature for which, with simulations longer than several $\mu$s, it is possible to equilibrate configurations in metastable equilibrium. More specifically, we have focused on the structural and topological changes taking place at the LL transition, supported by the possibility to contrast two 25 $\mu$s runs with the same temperature and pressure but different density.

We have capitalized on the possibility to define unambiguously the existing HBs, a possibility offered by the low $T$ at which the LL transition takes place, improved by the minimization procedure that eliminates vibrational distortion. The important result is the observation that on both sides of the transition, essentially all H atoms are involved in HBs. Again, this is a result enforced by the low $T$, which makes the loss of an HB (with its characteristic energy significantly larger than the thermal energy) a rare event. The large majority of the possible HBs are distributed in the characteristic two-donor two-acceptor tetrahedral state, with a minority of (equally numerous) three- and five-coordinated particles. The formation of these network defect pairs preserves the total number of HB, and it has thus a relatively minor energetic cost. At coexistence, both low and high density water can be described as a network of (mostly) four-coordinated molecules.

Finally, we have analyzed the changes in the H-bond network across the transition with the aim of better understanding the structural origin of the transition itself. Indeed, there is consensus (supported by experimental neutron and x-ray measurements in the high- and low-density amorphous structures)[26] that the dominant structural change between low- and high-density amorphous ice is the presence of interstitial molecules at high density located around $r \approx 0.35$ nm, in between the first and second shells of the structure expected for a random tetrahedral network. These interstitial molecules have been thought to originate from the collapse of the second shell. By partitioning the radial distribution function in contributions associated with different chemical distances (defined as the number of HBs separating two molecules) and at an even more sophisticated level separating each chemical distance in contributions arising from rings of different lengths, we have been able to show that the "typical" interstitial molecule is tetrahedrally coordinated and is connected to the central molecule by chemical distances rarely of 2 (these ones associated with the formation of rings of length 4) but mostly 3 and 4. Thus, rings of length 7 and longer adopt folded and elongated shapes to bring two molecules on opposite ring-sides close-by in space. The presence of these folded long

rings constitutes a characteristic property of the high-density liquid phase.

Pairs of molecules at the interstitial distance $r \approx 0.35$ nm connected by these long rings have both distinct and well-defined first and quite often also second bond-coordination shells. In other words, the two close-by molecules facing each other can be considered the starting points of two tetrahedral networks, which retain their independence up to the second generation and which grow on opposite sides, as if repelling each other, as vividly shown in Fig. 12.

The results presented in this paper demonstrate that the network topology contains the information for deciphering the structural differences between the low- and high-density liquids, and their significance also naturally extends to the description of low- and high-density amorphous forms of water, these glasses being—in the presence of a LL critical point—the LDL and HDL arrested counterparts. The results shown in Fig. 11 make clear that well-defined peaks in the radial distribution function of the HDL phase can be discerned once the contributions are separated on the basis of ring lengths and chemical distances. This offers the possibility to identify local structures, which are unambiguously part of the HDL state. Future work may indicate if this classification can be extended to supercritical conditions up to ambient temperature and pressure.

Finally, we note that particle-rings of length 8 (defined as described in Sec. III A) exist only in the HDL phase. An order parameter to investigate the nucleation of one liquid phase into the other one could possibly be designed on the basis of the present observation.

## SUPPLEMENTARY MATERIAL

See the supplementary material for additional data and application of the structural–topological analysis to the real dynamics of water.

## ACKNOWLEDGMENTS

J.R. acknowledges the support from the European Research Council, Grant No. DLV-759187. F.S. and R.F. acknowledge the support from MIUR-PRIN (Grant No. 2017Z55KCW).

## DATA AVAILABILITY

The data that support the findings of this study are available within the article and its supplementary material. Additional data (GROMACS input files) are available from the corresponding author upon reasonable request.

## REFERENCES

[1]K. Amann-Winkel, C. Gainaru, P. H. Handle, M. Seidl, H. Nelson, R. Böhmer, and T. Loerting, "Water's second glass transition," Proc. Natl. Acad. Sci. U. S. A. **110**, 17720 (2013).

[2]M. E. M. Azouzi, C. Ramboz, J.-F. Lenain, and F. Caupin, "A coherent picture of water at extreme negative pressure," Nat. Phys. **9**, 38 (2013).

[3]F. Perakis, K. Amann-Winkel, F. Lehmkühler, M. Sprung, D. Mariedahl, J. A. Sellberg, H. Pathak, A. Späh, F. Cavalca, D. Schlesinger *et al.*, "Diffusive dynamics during the high-to-low density transition in amorphous ice," Proc. Natl. Acad. Sci. U. S. A. **114**, 8193 (2017).

[4]K. H. Kim, A. Späh, H. Pathak, F. Perakis, D. Mariedahl, K. Amann-Winkel, J. A. Sellberg, J. H. Lee, S. Kim, J. Park *et al.*, "Maxima in the thermodynamic response and correlation functions of deeply supercooled water," Science **358**, 1589 (2017).

[5]J. N. Stern, M. Seidl-Nigsch, and T. Loerting, "Evidence for high-density liquid water between 0.1 and 0.3 GPa near 150 K," Proc. Natl. Acad. Sci. U. S. A. **116**, 9191 (2019).

[6]K. H. Kim, K. Amann-Winkel, N. Giovambattista, A. Späh, F. Perakis, H. Pathak, M. L. Parada, C. Yang, D. Mariedahl, T. Eklund, T. J. Lane, S. You, S. Jeong, M. Weston, J. H. Lee, I. Eom, M. Kim, J. Park, S. H. Chun, P. H. Poole, and A. Nilsson, "Experimental observation of the liquid-liquid transition in bulk supercooled water under pressure," Science **370**, 978 (2020).

[7]L. Kringle, W. A. Thornley, B. D. Kay, and G. A. Kimmel, "Reversible structural transformations in supercooled liquid water from 135 to 245 K," Science **369**, 1490 (2020).

[8]P. H. Poole, F. Sciortino, U. Essmann, and H. E. Stanley, "Phase behaviour of metastable water," Nature **360**, 324 (1992).

[9]M. Yamada, S. Mossa, H. E. Stanley, and F. Sciortino, "Interplay between time-temperature transformation and the liquid-liquid phase transition in water," Phys. Rev. Lett. **88**, 195701 (2002).

[10]Y. Li, J. Li, and F. Wang, "Liquid–liquid transition in supercooled water suggested by microsecond simulations," Proc. Natl. Acad. Sci. U. S. A. **110**, 12209 (2013).

[11]Y. Ni and J. L. Skinner, "Evidence for a liquid-liquid critical point in supercooled water within the E3B3 model and a possible interpretation of the kink in the homogeneous nucleation line," J. Chem. Phys. **144**, 214501 (2016).

[12]P. H. Handle and F. Sciortino, "Potential energy landscape of TIP4P/2005 water," J. Chem. Phys. **148**, 134505 (2018).

[13]T. E. Gartner, L. Zhang, P. M. Piaggi, R. Car, A. Z. Panagiotopoulos, and P. G. Debenedetti, "Signatures of a liquid–liquid transition in an ab initio deep neural network model for water," Proc. Natl. Acad. Sci. U. S. A. **117**, 26040 (2020).

[14]Y. Liu, J. C. Palmer, A. Z. Panagiotopoulos, and P. G. Debenedetti, "Liquid-liquid transition in ST2 water," J. Chem. Phys. **137**, 214505 (2012).

[15]F. Sciortino, I. Saika-Voivod, and P. H. Poole, "Study of the ST2 model of water close to the liquid–liquid critical point," Phys. Chem. Chem. Phys. **13**, 19759 (2011).

[16]T. A. Kesselring, G. Franzese, S. V. Buldyrev, H. J. Herrmann, and H. E. Stanley, "Nanoscale dynamics of phase flipping in water near its hypothesized liquid-liquid critical point," Sci. Rep. **2**, 474 (2012).

[17]J. C. Palmer, F. Martelli, Y. Liu, R. Car, A. Z. Panagiotopoulos, and P. G. Debenedetti, "Metastable liquid-liquid transition in a molecular model of water," Nature **510**, 385 (2014).

[18]P. G. Debenedetti, F. Sciortino, and G. H. Zerze, "Second critical point in two realistic models of water," Science **369**, 289 (2020).

[19]C. Vega, J. L. F. Abascal, M. M. Conde, and J. L. Aragones, "What ice can teach us about water interactions: A critical comparison of the performance of different water models," Faraday Discuss. **141**, 251 (2009).

[20]J. L. F. Abascal and C. Vega, "A general purpose model for the condensed phases of water: TIP4P/2005," J. Chem. Phys. **123**, 234505 (2005).

[21]J. L. F. Abascal, E. Sanz, R. García Fernández, and C. Vega, "A potential model for the study of ices and amorphous water: TIP4P/Ice," J. Chem. Phys. **122**, 234511 (2005).

[22]H. Tanaka, "Liquid–liquid transition and polyamorphism," J. Chem. Phys. **153**, 130901 (2020).

[23]C. G. Salzmann, "Advances in the experimental exploration of water's phase diagram," J. Chem. Phys. **150**, 060901 (2019).

[24]P. H. Handle, T. Loerting, and F. Sciortino, "Supercooled and glassy water: Metastable liquid(s), amorphous solid(s), and a no-man's land," Proc. Natl. Acad. Sci. U. S. A. **114**, 13336 (2017).

[25]P. Gallo, K. Amann-Winkel, C. A. Angell, M. A. Anisimov, F. Caupin, C. Chakravarty, E. Lascaris, T. Loerting, A. Z. Panagiotopoulos, J. Russo *et al.*, "Water: A tale of two liquids," Chem. Rev. **116**, 7463 (2016).

[26]K. Amann-Winkel, R. Böhmer, F. Fujara, C. Gainaru, B. Geil, and T. Loerting, "Colloquium: Water's controversial glass transitions," Rev. Mod. Phys. **88**, 011002 (2016).

[27]M. J. Abraham, T. Murtola, R. Schulz, S. Páll, J. C. Smith, B. Hess, and E. Lindahl, "GROMACS: High performance molecular simulations through multi-level parallelism from laptops to supercomputers," SoftwareX **1-2**, 19 (2015).
[28]F. H. Stillinger, *Energy Landscapes, Inherent Structures, and Condensed-Matter Phenomena* (Princeton University Press, 2015).
[29]F. Sciortino, "Potential energy landscape description of supercooled liquids and glasses," J. Stat. Mech: Theory Exp. **2005**, P05015.
[30]E. Whalley, D. D. Klug, and Y. P. Handa, "Entropy of amorphous ice," Nature **342**, 782 (1989).
[31]R. Shi, J. Russo, and H. Tanaka, "Common microscopic structural origin for water's thermodynamic and dynamic anomalies," J. Chem. Phys. **149**, 224502 (2018).
[32]T. A. Weber and F. H. Stillinger, "Removing chemical bonding ambiguities in condensed media by steepest-descent quenching," J. Chem. Phys. **87**, 3252 (1987).
[33]A. Luzar and D. Chandler, "Hydrogen-bond kinetics in liquid water," Nature **379**, 55 (1996).
[34]I. M. Svishchev and P. G. Kusalik, "Structure in liquid water: A study of spatial distribution functions," J. Chem. Phys. **99**, 3049 (1993).
[35]P. G. Kusalik and I. M. Svishchev, "The spatial structure in liquid water," Science **265**, 1219 (1994).
[36]R. Kumar, J. R. Schmidt, and J. L. Skinner, "Hydrogen bonding definitions and dynamics in liquid water," J. Chem. Phys. **126**, 204107 (2007).
[37]H. E. Stanley and J. Teixeira, "Interpretation of the unusual behavior of $H_2O$ and $D_2O$ at low temperatures: Tests of a percolation model," J. Chem. Phys. **73**, 3404 (1980).
[38]A. Geiger, F. H. Stillinger, and A. Rahman, "Aspects of the percolation process for hydrogen-bond networks in water," J. Chem. Phys. **70**, 4185 (1979).
[39]A. Geiger and H. E. Stanley, "Tests of universality of percolation exponents for a three-dimensional continuum system of interacting waterlike particles," Phys. Rev. Lett. **49**, 1895 (1982).
[40]F. Sciortino and S. L. Fornili, "Hydrogen bond cooperativity in simulated water: Time dependence analysis of pair interactions," J. Chem. Phys. **90**, 2786 (1989).
[41]F. Sciortino, A. Geiger, and H. E. Stanley, "Effect of defects on molecular mobility in liquid water," Nature **354**, 218 (1991).
[42]P. H. Poole, S. R. Becker, F. Sciortino, and F. W. Starr, "Dynamical behavior near a liquid–liquid phase transition in simulations of supercooled water," J. Phys. Chem. B **115**, 14176 (2011).
[43]D. Laage and J. T. Hynes, "A molecular jump mechanism of water reorientation," Science **311**, 832 (2006).
[44]S. Saito, B. Bagchi, and I. Ohmine, "Crucial role of fragmented and isolated defects in persistent relaxation of deeply supercooled water," J. Chem. Phys. **149**, 124504 (2018).
[45]J. M. Montes de Oca, F. Sciortino, and G. A. Appignanesi, "A structural indicator for water built upon potential energy considerations," J. Chem. Phys. **152**, 244503 (2020).
[46]P. A. Giguère, "The bifurcated hydrogen-bond model of water and amorphous ice," J. Chem. Phys. **87**, 4835 (1987).
[47]J.-P. Hansen and I. R. McDonald, *Theory of Simple Liquids: With Applications of Soft Matter* (Elsevier, Academic Press, Amsterdam, 2013).
[48]R. Shi and H. Tanaka, "Direct evidence in the scattering function for the coexistence of two types of local structures in liquid water," J. Am. Chem. Soc. **142**, 2868 (2020).
[49]A. Nilsson and L. Pettersson, "The structural origin of anomalous properties of liquid water," Nat. Commun. **6**, 8998 (2015).
[50]H. Tanaka, H. Tong, R. Shi, and J. Russo, "Revealing key structural features hidden in liquids and glasses," Nat. Rev. Phys. **1**, 333 (2019).
[51]A. K. Soper and M. A. Ricci, "Structures of high-density and low-density water," Phys. Rev. Lett. **84**, 2881 (2000).
[52]L. B. Skinner, M. Galib, J. L. Fulton, C. J. Mundy, J. B. Parise, V.-T. Pham, G. K. Schenter, and C. J. Benmore, "The structure of liquid water up to 360 MPa from x-ray diffraction measurements using a high Q-range and from molecular simulation," J. Chem. Phys. **144**, 134504 (2016).
[53]D. Mariedahl, F. Perakis, A. Späh, H. Pathak, K. H. Kim, G. Camisasca, D. Schlesinger, C. Benmore, L. G. M. Pettersson, A. Nilsson, and K. Amann-Winkel, "X-ray scattering and O–O pair-distribution functions of amorphous ices," J. Phys. Chem. B **122**, 7616 (2018).
[54]A. Rahman and F. H. Stillinger, "Hydrogen-bond patterns in liquid water," J. Am. Chem. Soc. **95**, 7943 (1973).
[55]R. J. Speedy, J. D. Madura, and W. L. Jorgensen, "Network topology in simulated water," J. Phys. Chem. **91**, 909 (1987).
[56]B. Santra, R. A. DiStasio, F. Martelli, and R. Car, "Local structure analysis in *ab initio* liquid water," Mol. Phys. **113**, 2829 (2015).
[57]G. Camisasca, D. Schlesinger, I. Zhovtobriukh, G. Pitsevich, and L. G. M. Pettersson, "A proposal for the structure of high- and low-density fluctuations in liquid water," J. Chem. Phys. **151**, 034508 (2019).
[58]M. Formanek and F. Martelli, "Probing the network topology in network-forming materials: The case of water," AIP Adv. **10**, 055205 (2020).
[59]R. Martoňák, D. Donadio, and M. Parrinello, "Evolution of the structure of amorphous ice: From low-density amorphous through high-density amorphous to very high-density amorphous ice," J. Chem. Phys. **122**, 134501 (2005).
[60]H. Pathak, A. Späh, K. H. Kim, I. Tsironi, D. Mariedahl, M. Blanco, S. Huotari, V. Honkimäki, and A. Nilsson, "Intermediate range O–O correlations in supercooled water down to 235 K," J. Chem. Phys. **150**, 224506 (2019).